

1.9 UPDATE ON WRF-ARW END-TO-END MULTI-SCALE FDDA SYSTEM

Aijun Deng^{*1}, David Stauffer¹, Brian Gaudet¹, Jimy Dudhia², Joshua Hacker², Cindy Bruyere², Wanli Wu², Francois Vandenberghe², Yubao Liu² and Al Bourgeois²

¹Penn State University, University Park, PA, USA

²National Center for Atmospheric Research, Boulder, CO, USA

1. INTRODUCTION

It is well known that nudging four-dimensional data assimilation (FDDA) is an effective and efficient way to reduce model errors (Stauffer and Seaman 1990). The nudging technique has several major uses. Firstly, it can be used to create four-dimensional dynamically consistent datasets (e.g., Deng et al. 2004, Deng and Stauffer 2006, Stauffer et al. 2007a, Schroeder et al. 2006, Zielonka and Stauffer 2008). Secondly, it can also be used to create improved lateral boundary conditions for process studies (e.g., Reen et al. 2006). Finally, it can be used for dynamic initialization, where the model is relaxed towards observed conditions during a pre-forecast period to improve the initial state and the subsequent short-term forecast (e.g., Stauffer et al. 2007a, b, Leidner et al. 2001, Otte et al. 2001).

During the last several years, Penn State led the implementation and testing of a prototype version of the three-dimensional (3D) analysis nudging FDDA capability that was originally released in WRFV2.2 in late 2006 (Deng et al. 2007, Deng et al. 2008). The analysis nudging can be used to assimilate 3D WRF native-coordinate gridded analyses of the u and v wind components, potential temperature, and mixing ratio. Similarly, a basic capability of observation nudging based on the Penn State MM5 observation nudging system was implemented at NCAR and was released to the public in WRFV2.2 (Liu et al. 2008).

Under the funding support of the Defense Threat Reduction Agency (DTRA), Penn State and NCAR have been working together to continue to improve the basic capabilities in both analysis and observation nudging FDDA in WRF-ARW. Under the DTRA FDDA contract through Penn State, a surface analysis nudging

capability has also been implemented in WRF-ARW to make use of higher temporal resolution surface analyses within the planetary boundary layer (PBL), and has been released to the public as part of the WRFV3.1 release in April 2009. As in MM5, this capability also accounts for data-analysis confidence by using the locations of observations that were used to produce the surface analyses in the calculation of the nudging weighting functions within the PBL. The 10-m observed wind is also scaled to the lowest model layer using similarity theory as in Stauffer et al. 1991. For surface moisture nudging, restrictions are applied to the analysis as in MM5 so that nudging to a supersaturated state is avoided.

Under the same DTRA contract, Penn State is working with NCAR to expand the flexibility of the WRF observation nudging to include options often used at Penn State for MM5 observation nudging. These include height-level based observations, additional space and time weighting factors for surface observations, additional options for vertical spreading of surface data and anisotropic horizontal weighting functions in the vicinity of terrain, improved quality control (QC) at finer vertical resolution for FDDA observation data sets, etc. One goal is to build an end-to-end FDDA system that includes all data preprocessing modules and the post-verification system. The flow chart of the end-to-end system is illustrated in Figure 1.

To easily produce analyses for use in WRF analysis nudging, and QC'ed observations for observation nudging, a new objective analysis capability called OBSGRID, has been developed at NCAR. The input to OBSGRID is the WRF Preprocessing System (WPS)/METGRID first-guess gridded output plus the decoded/reformatted observational data, such as upper air soundings and surface obs, in the MM5 little_r data format. The output from OBSGRID includes 1) the gridded, 3D, analyzed fields that are processed by REAL to prepare initial conditions, lateral boundary conditions and 3D analysis nudging input files, 2) gridded surface

**Corresponding author address:*

Aijun Deng, Department of Meteorology, 503 Walker Building, Pennsylvania State University, University Park, PA 16802-5013, email: deng@meteo.psu.edu

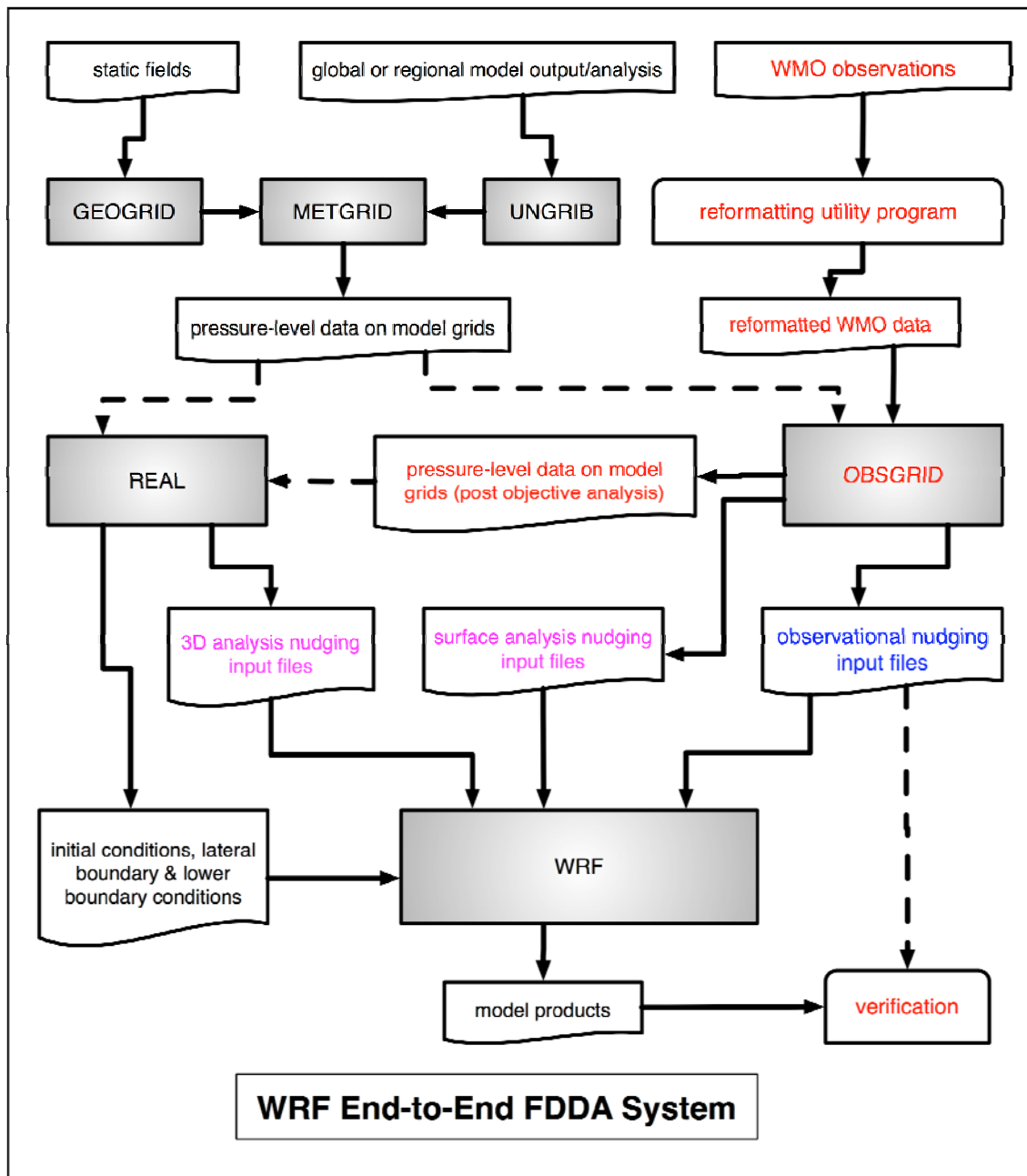


Figure 1. WRF end-to-end FDDA system. New FDDA capabilities are highlighted in red. The observational FDDA input files are shown in blue and the analysis FDDA files are shown in magenta.

analyses to be used directly by the WRF surface analysis nudging, and 3) QC'ed observations to be used directly by the WRF observation nudging. At the end of the system, a verification module that uses observations from OBSGRID as input can be used for WRF model output verification.

This paper presents our latest WRF results that use both analysis nudging and observation nudging in a multiscale FDDA configuration (Stauffer and Seaman 1994), based on two case

studies. The first case is from the CAPTEX-83 field experiment, where a grid configuration of 36-/12-/4-km in horizontal and 32 model layers in vertical are used and WRF IC/LBCs are converted from the MM5 RAWINS. Thus, no WRF WPS processing is involved such that model results only reflect the FDDA design within the WRF model itself. The second case is chosen from a winter case over the region around Alaska where WRF is configured to use a 12-/4-km grid configuration and very high

vertical resolution in the lower PBL (with 2-, 6-, 10-m, etc. vertical level heights). The second case is used to demonstrate the end-to-end FDDA system that involves all the steps illustrated in Figure 1 including WPS and OBSGRID.

2. METHODOLOGY

In nudging FDDA, the model state is relaxed continuously toward the observed state at each time step by adding an artificial tendency term, which is based on the difference between the two states, to the prognostic equations. Stauffer and Seaman (1990, 1994) suggest that the assimilation can be accomplished by nudging the model solutions toward gridded analyses based on observations (analysis nudging), or directly toward the individual observations (observation nudging), with an effective multiscale grid-nesting assimilation method using a combination of these two approaches.

In analysis nudging, the model fields are nudged at every grid point toward an analysis of the observations on the model grid in a manner such that the nudging term is proportional to the difference between the model and the analysis at each grid point. In observation nudging, the model solution is nudged toward the observations within the given radius of influence near the observation locations, and within the given time window surrounding the observations.

The nudging term should be smaller in magnitude than any of the other terms in the equations so that the nudging term does not control the tendency. If the nudging is too strong, the model may lose important mesoscale features created by the model, but if it is too weak, the observations will have a minimal effect on the evolution of the model state, allowing phase and amplitude errors to grow. For this reason, the value of the nudging factor should be carefully defined.

In the current version of the analysis nudging in WRF-ARW (WRFV3.1), the following equation represents a nudging term for potential temperature or any general predictive variable in WRF coupled with the dry hydrostatic pressure μ , where

$$\Theta = \mu \cdot \theta \quad (1)$$

and the prognostic equation including the nudging terms becomes

$$\begin{aligned} \frac{\partial \Theta}{\partial t} &= \dots + \mu \frac{\partial \theta}{\partial t} + \theta \frac{\partial \mu}{\partial t} \\ &= \dots + \mu \cdot G_{\theta} \cdot W \cdot (\theta_{ob} - \theta) + \theta \cdot G_{\mu} \cdot W \cdot (\mu_{ob} - \mu) \end{aligned} \quad (2)$$

where the four-dimensional weighting function is given by $W = w_{xy} \cdot w_{\eta} \cdot w_t$, the nudging coefficient is G , and $1/G$ is the e-folding time, which is a representative time scale for the artificial nudging term. This time scale should be longer than the time scale of the slowest physical process in the model. WRF-ARW uses μ in its terrain following vertical coordinate η , similar to the way total basestate pressure was used in the hydrostatic MM4/MM5 vertical σ coordinate. However, the WRF-ARW vertical coordinate surfaces (η) are not located at fixed heights independent of time as is the case in the nonhydrostatic MM5. Currently in WRF-ARW, both analysis nudging and observation nudging can be applied to u (west-east wind component), v (south-north wind component), θ (potential temperature), and q_v (water vapor mixing ratio). Nudging is not applied to μ .

3. EXPERIMENTAL DESIGN

To demonstrate the effectiveness of nudging FDDA in a multiscale framework, for both the CAPTEX-83 and Alaska cases, four sets of experiments are designed: 1) NOFDDA – control with no FDDA; 2) GFDDA – only 3D gridded analysis nudging and 3-hourly surface analysis nudging (the CAPTEX-83 cases does not involve surface analysis nudging); 3) OFDDA – only observation nudging; and 4) MFDDA – multi-scale FDDA with both analysis nudging and observation nudging.

Figure 2 shows the WRF 108/36/12/4-km grid configuration used for the CAPTEX-83 case that also uses the 32-layer configuration in the vertical, with the first model layer centered at about 30 m. Note that a 108-km grid existed for historical reasons but is not used in this study. As shown in Table 1, for the OFDDA experiment in the CAPTEX-83 case, only observation nudging is applied (no analysis nudging) on the 36- 12- and 4-km grids. In the GFDDA experiment, only analysis nudging (no observation nudging) is applied on all grids except the 4-km grid, with reduced nudging strength on the 12-km grid (see Table 2). In the MFDDA experiment, analysis nudging is used on the 36- and 12-km grids and observation nudging is applied on all grids. All the FDDA

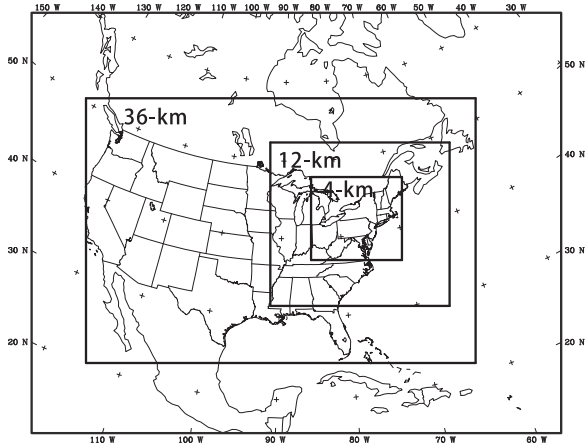


Figure 2: Captex-83 WRF 108/36/12/4-km grid configuration

parameters used in the CAPTEX-83 case are listed in Table 2. For both analysis nudging and observation nudging, nudging of wind fields is applied on all the model layers and nudging of mass fields is only applied above the model-simulated PBL. All CAPTEX-83 experiments use WRFV2.2.1, MYJ PBL scheme with the Penn State improvements (Deng et al. 2008), KF CPS on the 36- and 12-km grids, Dudhia SW and RRTM LW radiation schemes. No land surface model is used. The model top is set to 100 hPa in the CAPTEX-83 case.

In the Alaska case (see Figure 3 for the 12-/4-km grid configuration), very high vertical resolution (with half-layer heights of 2 m, 6 m, 10 m, etc.) is used, with 45 total model layers and a model top at 50 hPa.

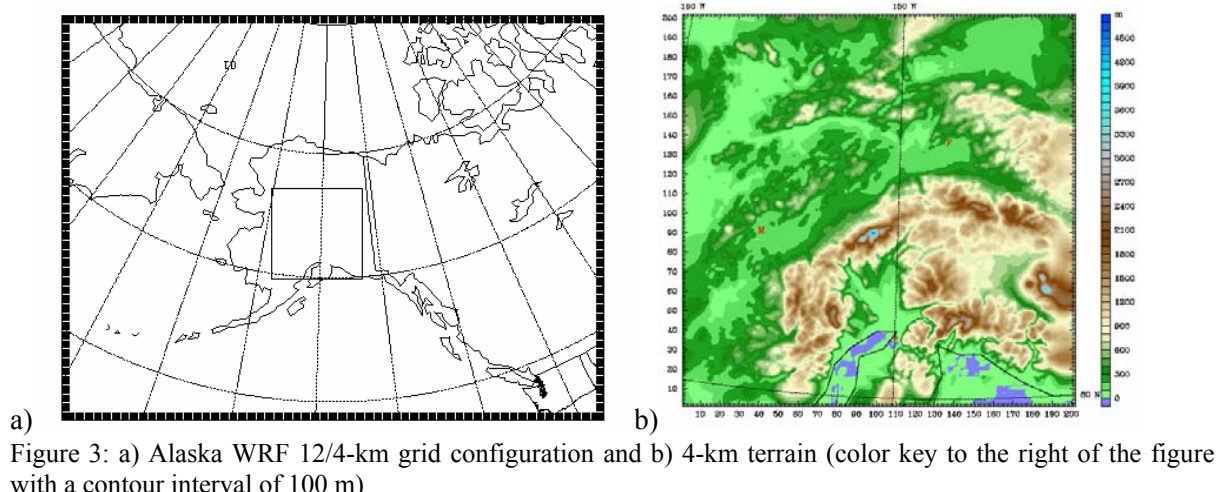
As shown in Table 3, for the Alaska case only observation nudging is applied (no analysis nudging) in the OFDDA experiment on both 12- and 4-km grids. In the GFDDA experiment, analysis nudging is applied on the 12-km grid only. In the MFDDA experiment, analysis nudging is used on the 12-km grids only, and observation nudging is applied on both grids. All the FDDA parameters used in the Alaska case are listed in Table 4. For both analysis nudging and observation nudging, nudging of both wind and mass fields is applied for all the model layers. In the Alaska case, surface analysis nudging is also used with the 3D analysis nudging to allow the use of 3-hourly surface analyses within the PBL (replacing 3D analysis nudging within the PBL). All Alaska experiments use WRFV3.1 Beta release, default MYJ PBL scheme (with reduced background TKE in some of the experiments), KF CPS on the 12-km grids, Dudhia SW and RRTM LW radiation schemes. The Noah land-surface model is also used.

Table 1: Multiscale FDDA experimental design for the CAPTEX-83 case

Exp. Name	36 km		12 km		4 km	
	3D Analysis Nudging	OBS Nudging	3D Analysis Nudging	OBS Nudging	3D Analysis Nudging	OBS Nudging
NOFDDA	NO	NO	NO	NO	NO	NO
OFDDA	NO	YES	NO	YES	NO	YES
GFDDA	YES	NO	YES	NO	NO	NO
MFDDA	YES	YES	YES	YES	NO	YES

Table 2: Multiscale FDDA parameters used in the CAPTEX-83 case

	3D Analysis Nudging			OBS Nudging		
	36km	12km	4km	36km	12km	4km
G (1/sec)	3×10^{-4}	1×10^{-4}	N/A	4×10^{-4}	4×10^{-4}	4×10^{-4}
Wind field	Nudging all layers	Nudging all layers	N/A	Nudging all layers	Nudging all layers	Nudging all layers
Mass field	Nudging above PBL	Nudging above PBL	N/A	Nudging above PBL	Nudging above PBL	Nudging above PBL
RINXY (km)	N/A	N/A	N/A	150	100	100
TWINDO (hr)	N/A	N/A	N/A	2	2	2
dt (sec)	N/A	N/A	N/A	180	60	20
IONF	N/A	N/A	N/A	2	4	10



4. PRELIMINARY RESULTS

1) CAPTEX-83

The model simulations for this case were performed using WRFV2.2.1. Figure 4 shows the MAE of WRF-simulated fields averaged in time over the entire 48-h model simulation period (starting at 12 UTC on 18 September 1983 and ending at 12 UTC on 20 September 1983) and for all model layers. It is clear that on the 36-km grid, for all model-simulated fields, both 3D analysis nudging only (GFDDA) and observation nudging only (OFDDA), significantly reduce model error. Analysis nudging shows a closer fit to observations than observation nudging. Combining the analysis nudging and observation nudging (MFDDA) further reduces model error. Similarly on the 12-km grid (again for all model simulated fields), both 3D analysis-nudging only and observation nudging only, significantly reduce model error, but observation nudging better fits the observations than analysis nudging, which is likely due to the observation nudging strength being greater than that in the analysis nudging (Table 2). On the 4-km grid, since no analysis nudging is directly used on this grid and thus it only affects this grid through the lateral boundary conditions, only observation nudging shows significant error reduction. Multiscale FDDA, which includes obs nudging on this grid and 3D analysis nudging on coarser grids, produces a comparable or slightly better fit to the observations compared to using observation nudging only. It is clear that multiscale FDDA produces the best fit to the observations over all three domains.

Table 3: Multiscale FDDA experimental design for Alaska case

Exp. Name	12 km		4 km	
	3D/Sfc Analysis Nudging	OBS Nudging	3D/Sfc Analysis Nudging	OBS Nudging
JOFDDA	NO	NO	NO	NO
OFDDA	NO	YES	NO	YES
GFDDA	YES	NO	NO	NO
MFDDA	YES	YES	NO	YES

Table 4: Multiscale FDDA parameters used in Alaska case

	3D / Sfc Analysis Nudging		OBS Nudging	
	12km	4km	12km	4km
G (1/sec)	3*10-4	N/A	4*10-4	4*10-4
Wind field	Nudging all layers	N/A	Nudging all layers	Nudging all layers
Mass field	Nudging all layers	N/A	Nudging all layers	Nudging all layers
RINXY (km)	N/A	N/A	100	100
TWINDO (hr)	N/A	N/A	2	2
dt (sec)	N/A	N/A	24	8
IONF	N/A	N/A	4	12

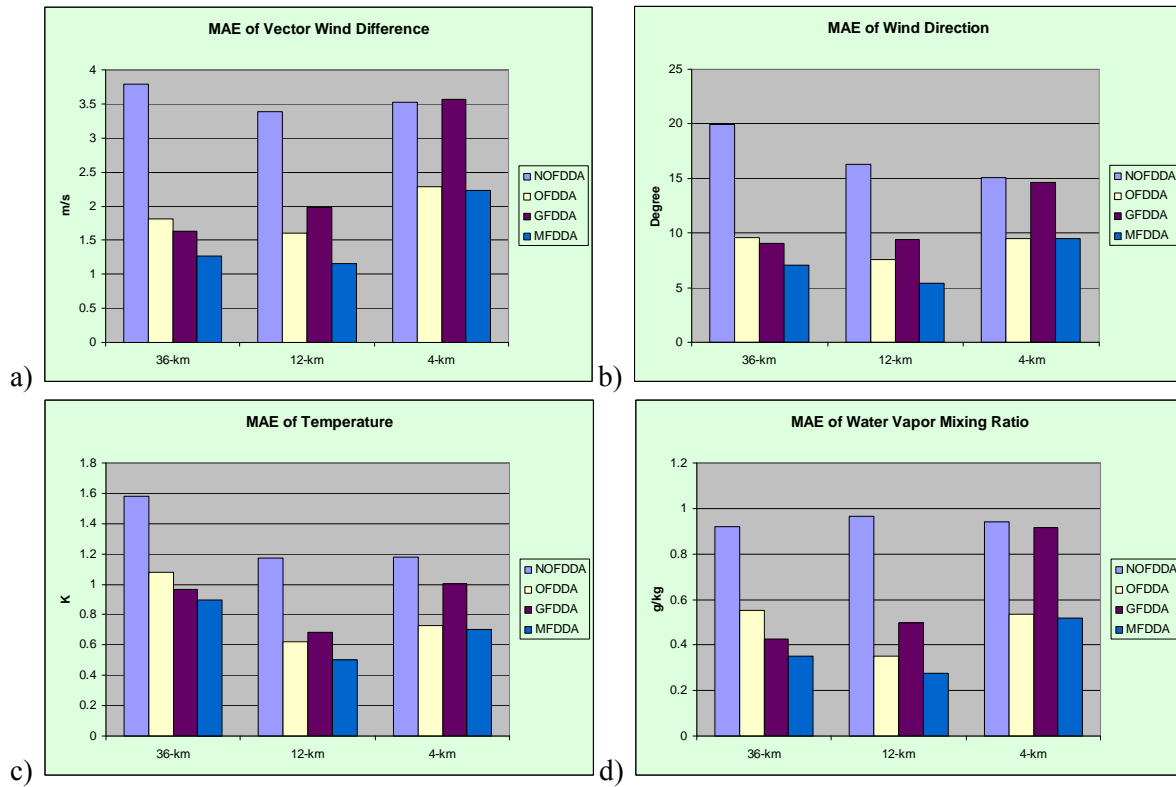


Figure 4. MAE of WRF-simulated fields averaged over time and all model layers for a) Vector Wind difference (m/s), b) Wind direction (degrees), c) Temperature (K), and d) Water vapor mixing ratio (g/kg) for the CAPTEX-83 case. The 48-hour WRF simulation starts at 12 UTC on 18 September 1983 and ends at 12 UTC on 20 September 1983.

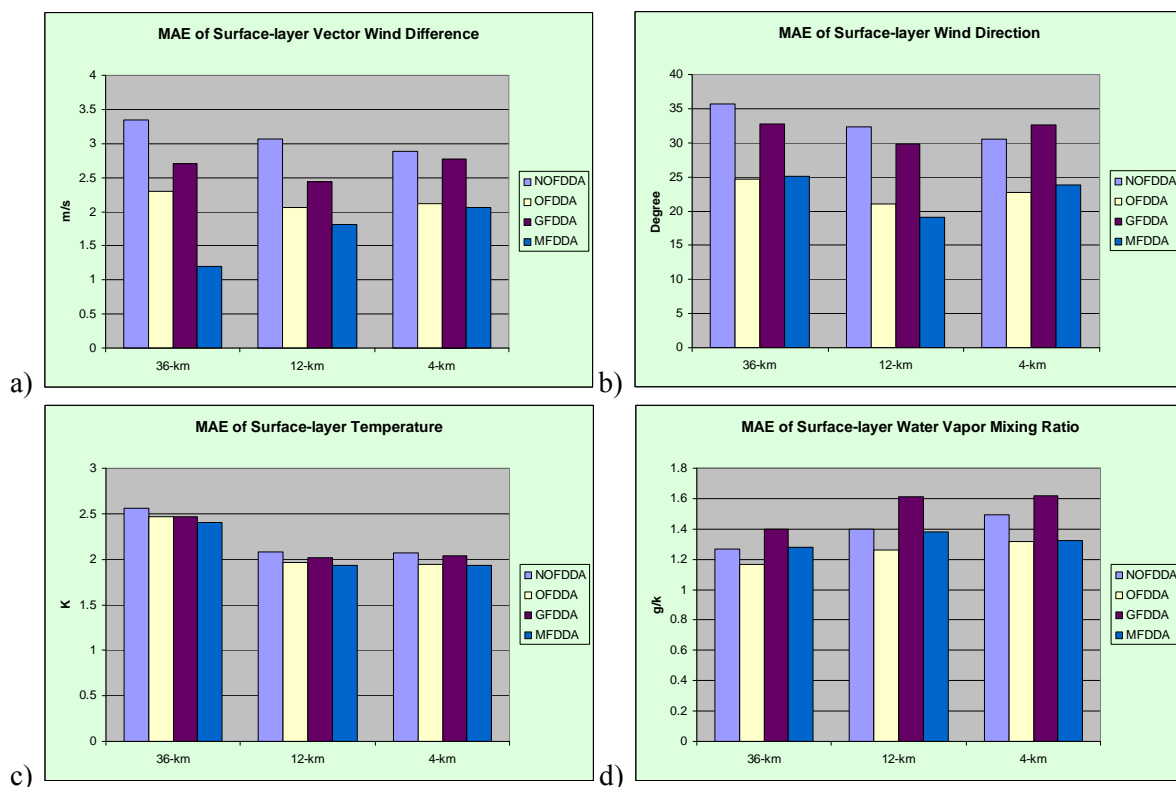


Figure 5. MAE of WRF-simulated surface layer fields averaged over the entire 48-h period for a) Vector Wind difference (m/s), b) Wind direction (degrees), c) Temperature (K), and d) Water vapor mixing ratio (g/kg) for the CAPTEX-83 case. The 48-h WRF simulation starts at 12 UTC on 18 September 1983 and ends at 12 UTC on 20 September 1983.

Figure 5 shows the MAE of WRF-simulated surface layer fields averaged in time over the entire 48-h model simulation period. No surface analysis nudging is used in this case, and as expected, we are seeing more error reduction in the surface layer due to observation nudging than analysis nudging for all fields and on all grids. Overall, for all domains and variables, multiscale FDDA again produces the best fit to the observations.

2) *Alaska-08*

The second case is a winter case over the Alaska region where WRF is configured to use very high vertical resolution in the lower planetary boundary layer (PBL). The 72-h model simulation starts at 00 UTC on 23 January 2008 and ends at 00 UTC on 26 January 2008. This case involves every step of the end-to-end WRF FDDA system, in which OBSGRID is used to create the gridded analyses needed for analysis nudging and QC'ed WMO observations needed for observation nudging. QC of WMO sounding observations is performed against the 26 pressure levels of the 0.5-degree GFS background (although QC performed over more vertical levels is desired in the future). The WRF model used for this case study is the WRFV3.1 pre-release which includes the surface analysis nudging capability. Thus in the Alaska case, we also expanded our original experimental design to include two additional experiments, GFDDAS – same as GFDDA but with surface analysis nudging included, and MFDDAS – same as MFDDA but with surface analysis nudging included. Note that analysis nudging is only used on the 12-km grid, not on the 4-km grid.

Figure 6 shows the RMS error of WRF-simulated wind and mass fields averaged over three 12 UTC (3 AM LST) times, verified against all WMO upper-air observations below the 750 hPa height level, for this Alaska case. Figure 7 shows the RMS error of WRF-simulated surface wind and mass fields averaged over the three 12 UTC times, verified against all WMO METAR stations. It is shown that the NOFDDA experiment generally has larger errors than either observation nudging only or 3D analysis nudging only; and the combination of observation nudging and 3D analysis nudging (i.e. MFDDA) is best overall (the exceptions are surface U and V on the 4-km grid, Fig. 7a and

7b, and note that only obs nudging produces larger error for V than NOFDDA for the surface). Statistical results with the surface analysis nudging (i.e. GFDDAS and MFDDAS) also suggest that there is some degradation for METAR-verified wind statistics, and especially for sounding-verified wind and temperature statistics below the 750 hPa height.

We hypothesize that several reasons could contribute to the degradation. First, since very high vertical resolution is used in the Alaska case, the innovation for surface wind (observed at 10 m AGL) is computed using the first model layer by default (which in this case is at 2 m) and applied through the entire PBL. This is definitely a problem and needs to be improved for high resolution applications, although it is not a problem in the normal case where the first model layer depth is greater than 10 m AGL (with the wind analysis scaled to the first model layer). For temperature, the surface analysis level and the first model layer are both at 2 m, which can explain why we are still seeing some improvements in the surface temperature RMSE (Fig. 7c).

Secondly, the more serious degradation in the upper-air RMS is likely due to the unexpectedly high PBL depths predicted by the WRF MYJ PBL scheme, since PBL height is used to determine how far the surface correction is extended vertically into the upper layers with the observation and surface analysis nudging schemes. Since this Alaska case uses the default MYJ PBL (which is shown to have a high PBL bias without Penn State improvements, Deng et al. 2008) it is not completely surprising to see the degradation. As a proof, Figure 8 shows the 4-km WRF-predicted PBL depth at 12 UTC (3 LST), 25 January 2008, in Experiment NOFDDA, which clearly shows some areas of unexpectedly large PBL depths (> 2 km) during the night (3 am). This issue can also be confirmed by the WRF-predicted time series of PBL depth shown in Figure 9, where a PBL depth of about 1.6 km is seen at Fairbanks at 12 UTC (3 LST), 25 January 2008. However, the model sounding at Fairbanks, Alaska at this time (Figure 10) shows a strong, deep inversion layer below 800 hPa that does not appear to support the PBL depth of 1.6 km that is used to vertically spread the surface nudging correction. Thirdly, it is possible that some uncertainties in the verification software using diagnosed 2-m (mass) and 10-m (wind) rather than the closest

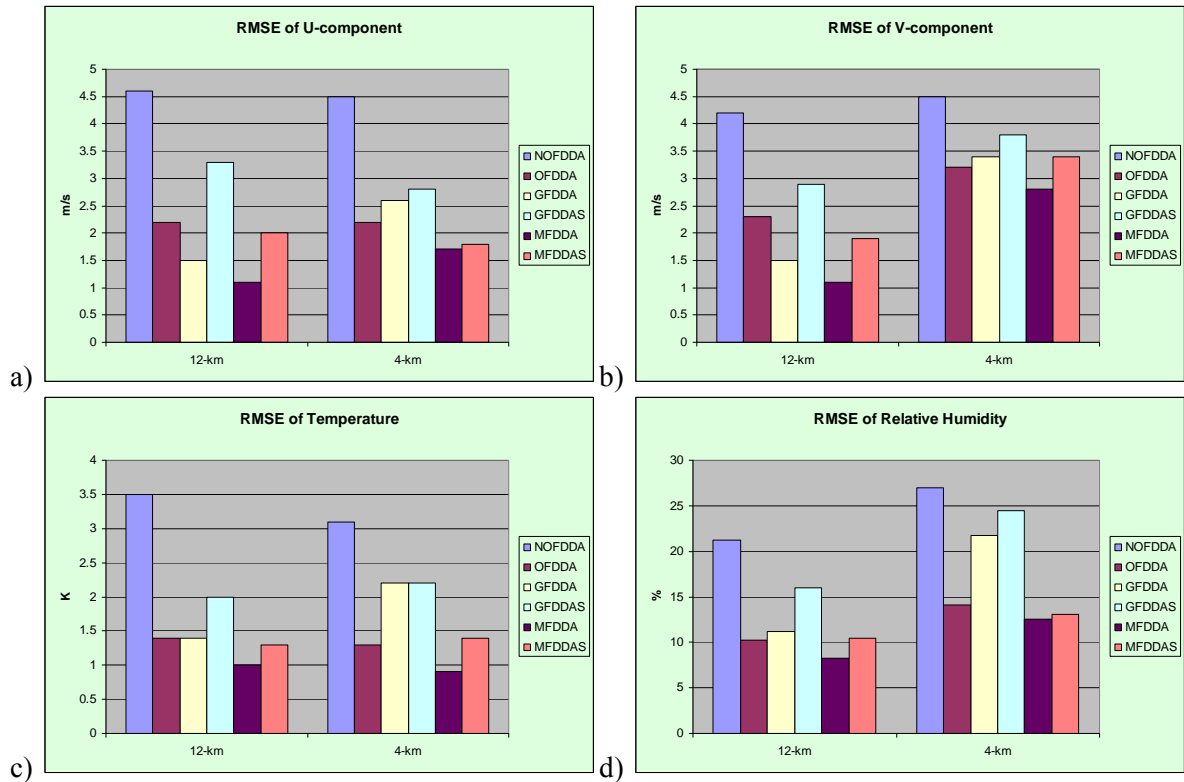


Figure 6. RMSE of WRF-simulated fields averaged over three 12 UTC (3 am LST) times and verified against sounding vertical levels from the surface to 750 hPa, for a) U-component (m/s), b) V-component, c) Temperature (K), and d) Relative Humidity (%) for the Alaska case. The 72-h WRF simulation starts at 00 UTC on 23 January 2008 and ends at 00 UTC on 26 January 2008.

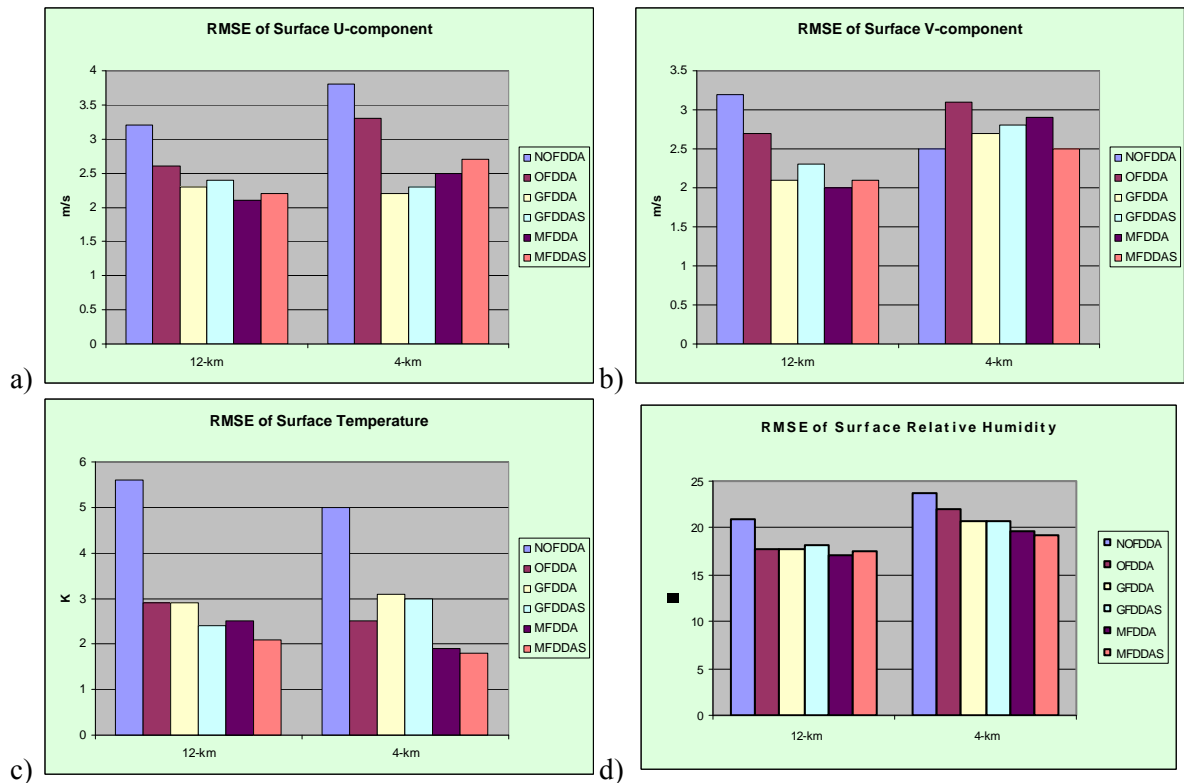


Figure 7. RMSE of WRF-simulated surface fields averaged over all three 12 UTC times and verified against surface METAR stations, for a) U-component (m/s), b) V-component, c) Temperature (K), and d) Relative Humidity (%) for the Alaska case. The 72-h WRF simulation starts at 00 UTC on 23 January 2008 and ends at 00 UTC on 26 January 2008.

Dataset: d02 RIP: realtime pbh Init: 0000 UTC Wed 23 Jan 08
 Post: 0000 h Valid: 1200 UTC Fri 25 Jan 08 (0300 LST Fri 25 Jan 08)
 PBL HEIGHT

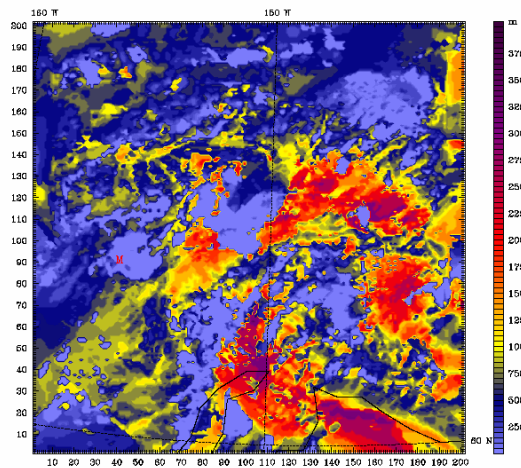


Figure 8. WRF-predicted PBL depth (m) on the 4-km domain at 12 UTC (03 LST), 25 January 2008 in Experiment NOFDDA.

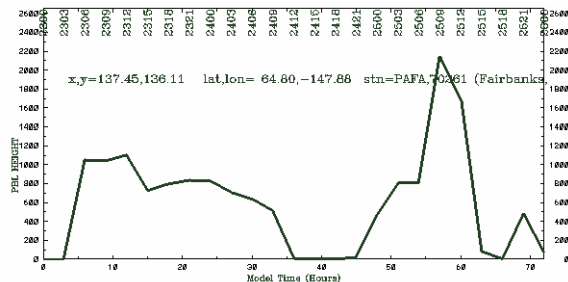


Figure 9. WRF-predicted PBL depth time series at Fairbanks, Alaska, on the 4-km domain starting at 00 UTC, 23 January 2008 and ending at 00 UTC, 26 January 2008 in Experiment NOFDDA.

Dataset: d01 RIP: realtime sonde01 Init: 0000 UTC Wed 23 Jan 08
 Post: 0000 h Valid: 1200 UTC Fri 25 Jan 08 (0300 LST Fri 25 Jan 08)
 Temperature x,y=201.48,151.04 lat,lon= 64.80,-147.88 stn=PAFA,70261
 Dewpoint temperature x,y=201.48,151.04 lat,lon= 64.80,-147.88 stn=PAFA,70261
 Horizontal wind vectors x,y=201.48,151.04 lat,lon= 64.80,-147.88 stn=PAFA,70261

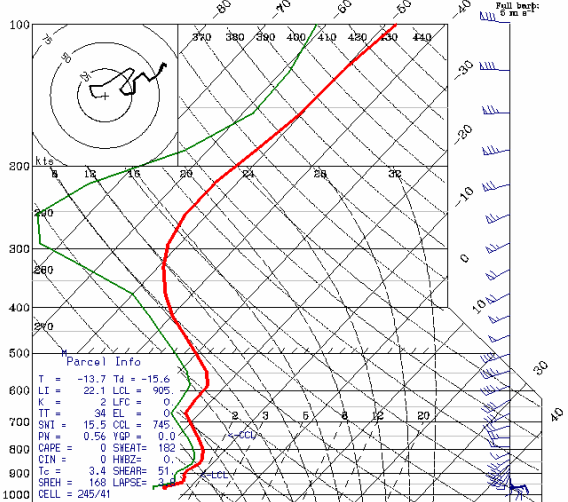


Figure 10. WRF-predicted sounding at Fairbanks, Alaska, on 4-km domain at 12 UTC (3 LST), 25 January 2008 in Experiment NOFDDA.

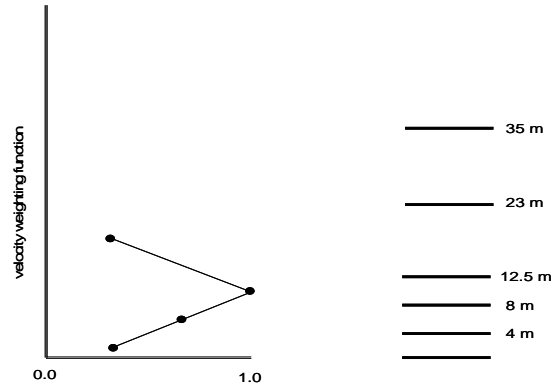


Figure 11 A simple weighting function used for the vertical spreading of surface observation of wind fields. Full layer levels for the Alaska configuration are shown by the thick lines at the right

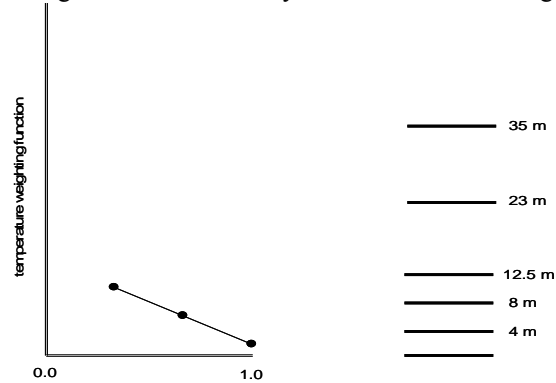


Figure 12 A simple weighting function used for the vertical spreading of surface observation of mass fields. Full layer levels for the Alaska configuration are shown by the thick lines at the right.

model layer may contribute to the elevated RMS scores.

It appears that to avoid model degradation, there is a need to improve the nudging strategy so that the vertical spreading of the surface obs is not solely dependent on the PBL depth. Other factors such as PBL regime should be used in addition to the PBL depth. We are currently working on a design plan for code improvement to address this issue for both obs nudging and analysis nudging. This plan will also address improving the nudging schemes used for cases with very high vertical resolution.

To verify that the high PBL depths predicted by the MYJ PBL scheme had contributed to the model FDDA degradation in the Alaska case with the current nudging strategy, as an alternative to the sophisticated design plan, a simple, hard-wired approach has been used in this Alaska case to define the surface data correction through the lowest several model layers. In this approach, as shown in Figs. 11 and 12, full weighting occurs at 2 m for T, q

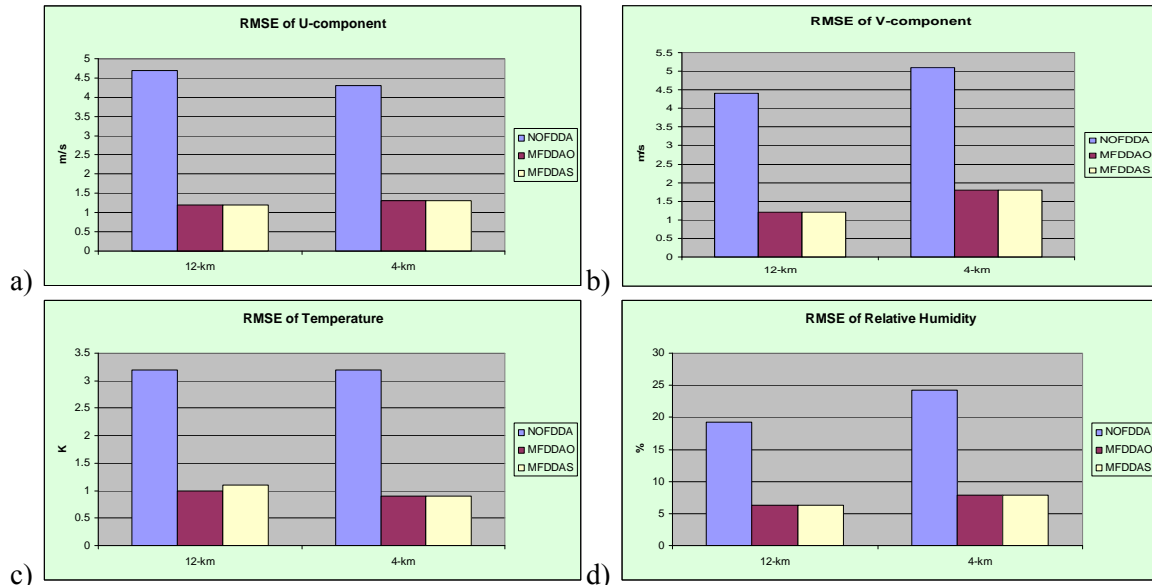


Figure 13 RMSE of WRF-simulated fields averaged over three 12 UTC times and verified against sounding vertical levels below 750 hPa, for a) U-component (m/s), b) V-component (m/s), c) Temperature (K), and d) Relative humidity (%) for the Alaska case. The 72-hour WRF simulation starts at 00 UTC on 23 January 2008 and ends at 00 UTC on 26 January 2008.

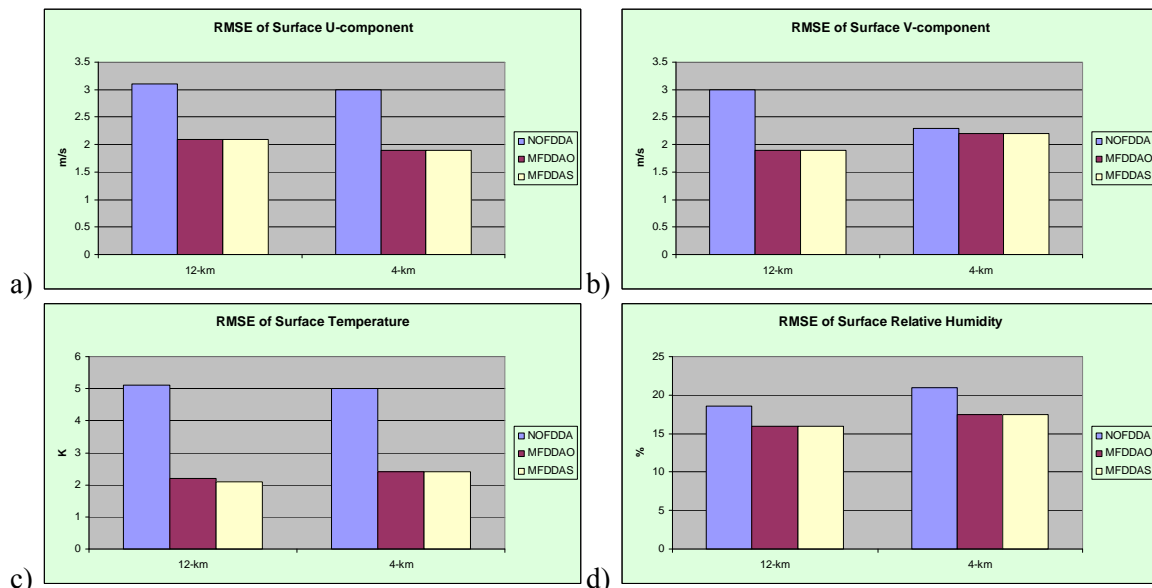


Figure 14 RMSE of WRF-simulated surface fields averaged over all three 12 UTC times and verified against surface METAR stations at k=3 (10 m) for a) U-component (m/s), b) V-component (m/s), and at k=1 (2 m) for c) Temperature (K), and d) Relative humidity (%) for the Alaska case. The 72-hour WRF simulation starts at 00 UTC on 23 January 2008 and ends at 00 UTC on 26 January 2008.

(corresponding with the first half-layer height) and 10 m for winds (corresponding closely to the third half-layer height). For T and q we use 0.667 weighting at the second half-layer at 6 m, 0.333 at the third half-layer at ~10 m, and 0 above. For winds, weighting is reduced to 0.667 and 0.333 at the second and first half-layer heights, respectively; moving upward, weights are reduced to 0.333 at the fourth half layer at ~18 m, and 0 at the fifth at 29 m and above.

Figures 13 and 14 show the RMSE of WRF-simulated fields (similar to Figs. 6 and 7) for three experiments: 1) NOFDDA – no FDDA is used, 2) MFDDAO – multiscale FDDA with modified observation nudging weights near surface as described above, and 3) MFDDAS – multiscale FDDA with modified surface analysis nudging weights near surface in addition to modified observation nudging weights. It is shown that both multiscale FDDA experiments significantly improve the model skills, and the

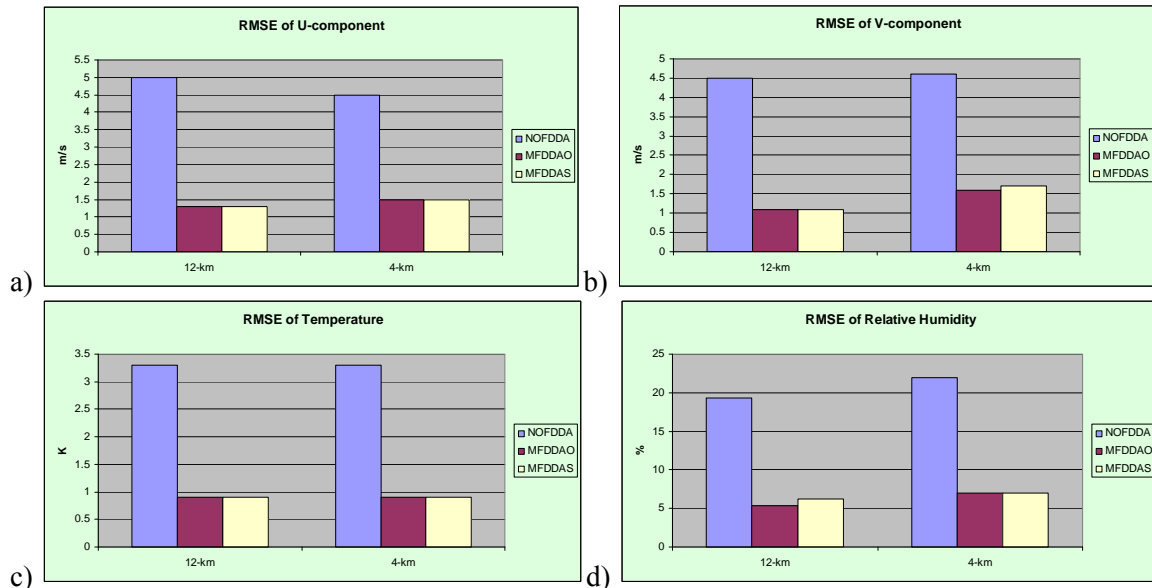


Figure 15. RMSE of WRF-simulated fields averaged over all 3-hourly times and verified against sounding vertical levels below 750 hPa, for a) U-component (m/s), b) V-component (m/s), c) Temperature (K), and d) Relative humidity (%) for the Alaska case. The 72-hour WRF simulation starts at 00 UTC on 23 January 2008 and ends at 00 UTC on 26 January 2008.

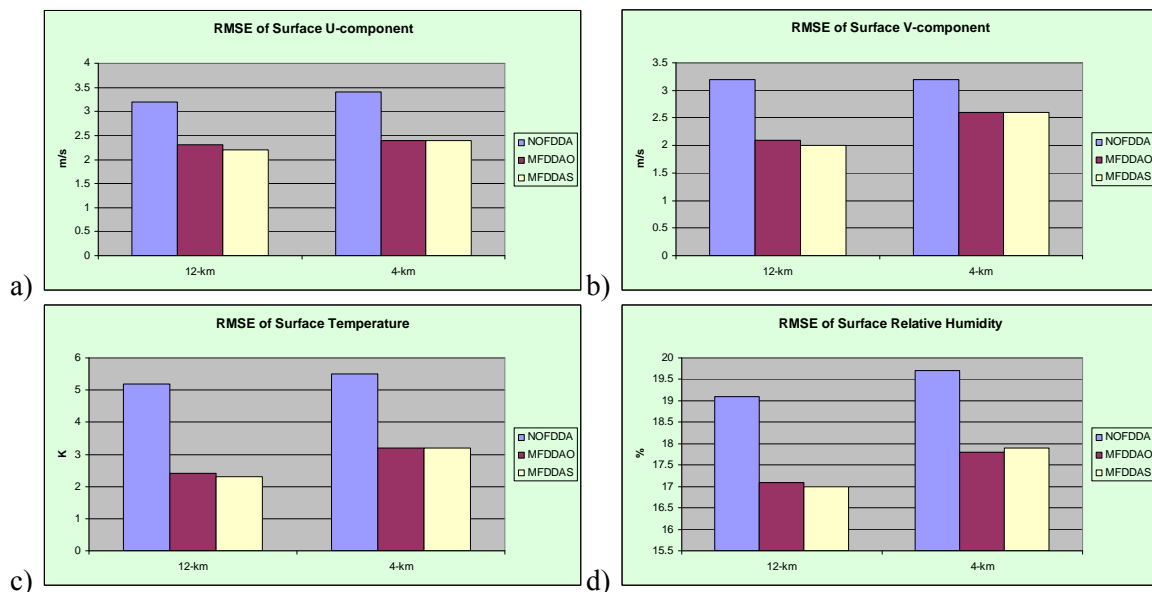


Figure 16 RMSE of WRF-simulated surface fields averaged over all 3-hourly times and verified against surface METAR stations, at k=3 (10 m) for a) U-component (m/s), b) V-component (m/s), and at k=1 (2 m) for c) Temperature (K), and d) Relative humidity (%) for the Alaska case. The 72-hour WRF simulation starts at 00 UTC on 23 January 2008 and ends at 00 UTC on 26 January 2008.

substantial degradation of model forecast skill due to surface-data nudging is no longer present.

The RMSE of WRF-simulated fields averaged over all 3-h times is shown for verification against soundings below 750 hPa in Fig. 15 and against surface observations in Fig. 16 (similar to Figs. 13 and 14, but those figures only show verification at the three 12 UTC times). Consistent with the 12 UTC verification, the 3 - h verification indicates that the use of

multiscale FDDA improves the RMSE of winds, temperature, and moisture both at the surface and below 750 hPa. Additionally, the modified surface analysis nudging weights generally decrease RMSE at the surface on the 12-km domain where surface analysis nudging was applied (compare 12-km MFDDAO and MFDDAS in Fig. 16).

To subjectively evaluate the performance of nudging FDDA in the Alaska case, Figs. 17, 18

closer fit to observations than observation nudging on the coarser 36-km grid, and observation nudging better fits the observations than analysis nudging on the 12-km grid where analysis nudging weights are defined to be much smaller. Multiscale FDDA, which includes both 3D analysis nudging and observation nudging on coarser domains, and only observation nudging on the 4-km domain, produces a comparable or slightly better fit to the observations on the 4-km domain compared to using observation nudging only. Multiscale FDDA produces the best fit to the observations over all three domains.

Penn State and NCAR have been working to build an end-to-end WRF FDDA system that includes all the data preprocessing modules and a post-verification system. Within the end-to-end system, in addition to 3D-VAR, a new objective analysis capability, called OBSGRID, has been developed at NCAR based on the MM5 RAWINS/little_r module. The input to OBSGRID is the WPS/METGRID first-guess gridded output and the decoded/reformatted observational data. The output from OBSGRID includes 1) the gridded 3D analyzed fields that are processed by REAL to prepare initial conditions, lateral boundary conditions and 3D analysis nudging input files, 2) gridded surface analyses to be used directly by the WRF surface analysis nudging, and 3) QC'ed observations to be used directly by the WRF observation nudging. At the end of the system, a verification module that uses observations from OBSGRID as input can be used for WRF model output verification.

The Alaska case is used to demonstrate the functionality of the end-to-end FDDA system and involves all the steps including the data preprocessing using OBSGRID as well as the verification module developed at NCAR. It was found that multiscale FDDA (combined 3D analysis and observation nudging on the 12-km domain, observation nudging on the 4-km domain) performed best overall at fitting the observations. However, there is some degradation, especially in the wind and temperature statistics below 750 hPa when the surface-data nudging is used, and a larger degradation is found in the upper air statistics rather than the surface. Further investigation that arbitrarily limits the surface correction to the lowest few model layers (instead of to the entire PBL) confirmed that the major degradation is caused by the large WRF-predicted PBL depths, and the FDDA correction from the surface data

assimilation being mixed to layers as high as 2 km during night time conditions.

Use of simplified vertical weights near the surface for surface-data nudging in observation nudging and surface analysis nudging caused large improvements in all variables compared to the NOFDDA control. There was also a slight improvement in the surface statistics for U, V, T and RH with the addition of surface analysis nudging to the observation nudging when verified at all 3-hourly times throughout the 72-h period.

Future work will include improving the nudging strategy so that the vertical spreading of the surface observations is not solely dependent on the PBL depth, but also dependent on other factors such as stability regime. Penn State is currently working on a sophisticated design plan for code improvements to address this issue for the surface analysis nudging and observation nudging as well. This plan will also include a strategy for improving nudging schemes used for cases with very high vertical resolution.

6. ACKNOWLEDGEMENTS

This research is supported by the Defense Threat Reduction Agency under contract no. HDTRA-1-07-C-0076 through Penn State under the supervision of John Hannan. The Alaska WRF modeling study is also supported by US EPA under contract no. EP08D000663 through Penn State under the supervision of Ken Schere and Jon Pleim. We also acknowledge Jeff Zielonka and Brian Reen of Penn State for their help in WRF verification for the Alaska case study.

7. REFERENCES

- Deng, A, N. L. Seaman, G. K. Hunter, and D. R. Stauffer, 2004: Evaluation of inter-regional transport using the MM5/SCIPUFF system. *J. Appl. Meteor.*, **43**, 1864-1886.
- Deng, A. and D.R. Stauffer, 2006: On improving 4-km mesoscale model simulations. *J. Appl. Meteor.*, **45**, 361-381.
- Deng, A., D.R. Stauffer, J. Dudhia, T.L. Otte, and G.K. Hunter, 2007: Update on analysis nudging FDDA in WRF-ARW, Preprints, *WRF Users' Workshop*, Boulder, CO, June 13, 9 pp.

- Deng, A., D.R. Stauffer, J. Dudhia, T.L. Otte, G.K. Hunter, and C. Bruyere, 2008: WRF-ARW analysis nudging update and future development plan, Preprints, *WRF Users' Workshop*, Boulder, CO, June 24, 8pp.
- Leidner, S.M., D.R. Stauffer and N.L. Seaman, 2001: Improving California coastal zone numerical weather prediction by dynamic initialization of the marine layer. *Mon. Wea. Rev.*, **129**, 275-294.
- Liu Y., A. Bourgeois, W. Wu, W. Yu, F. Vandenberghe, M. Xu, G. Roux, J. Dudhia, J. Hacker, T. Warner, S. Swerdlin, L. Lei, A. Deng, and D. R. Stauffer, 2008: WRF observation-nudging updates, verification and future development plans. 9th WRF Users Workshop, June 23-27, 2008, Boulder, CO.
- Otte, T.L. N.L. Seaman and D.R. Stauffer, 2001: A heuristic study on the importance of anisotropic error distributions in data assimilation. *Mon. Wea. Rev.*, **129**, 766-783.
- Reen, B. P., D. R. Stauffer, K. J. Davis, and A. R. Desai, 2006: A Case Study on the Effects of Heterogeneous Soil Moisture on Mesoscale Boundary-Layer Structure in the Southern Great Plains, U.S.A. Part II: Mesoscale Modelling. *Bound.-Layer Meteor.*, **120**, 275-314. DOI 10.1007/s10546-006-9056-6.
- Schroeder, A.J., D.R. Stauffer, N.L. Seaman, A. Deng, A.M. Gibbs, G.K. Hunter, and G.S. Young, 2006: An automated high-resolution, rapidly relocatable meteorological nowcasting and pre-diction system. *Mon. Wea. Rev.*, **134**, 1237-1265.
- Stauffer, D. R., and N. L. Seaman, 1990: Use of four-dimensional data assimilation in a limited-area mesoscale model. Part I: Experiments with synoptic-scale data. *Mon. Wea. Rev.*, **118**, 1250-1277.
- Stauffer, D. R., N. L. Seaman, and F. S. Binkowski, 1991: Use of four-dimensional data assimilation in a limited-area mesoscale model. Part II: Effects of data assimilation within the planetary boundary layer. *Mon. Wea. Rev.*, **119**, 734-754.
- Stauffer, D. R., and N.L. Seaman, 1994: On Multi-Scale Four-Dimensional Data Assimilation. *J. Appl. Meteor.*, **33**, 416-434.
- Stauffer, D.R., A. Deng, G.K. Hunter, A.M. Gibbs, J.R. Zielonka, K. Tinklepaugh, and J. Dobek, 2007a: NWP goes to war ..., 22nd Conference on Weather Analysis and Forecasting/18th Conference on Numerical Weather Prediction, June 25-29, Park City, UT.
- Stauffer, D.R., G.K. Hunter, A. Deng, J.R. Zielonka, K. Tinklepaugh, P. Hayes, and C. Kiley, 2007b: On the role of atmospheric data assimilation and model resolution on model forecast accuracy for the Torino Winter Olympics, 22nd Conference on Weather Analysis and Forecasting/18th Conference on Numerical Weather Prediction, June 25-29, Park City, UT.
- Zielonka, J.R. and D.R. Stauffer, 2008: A year-long gulf coast mesoscale modeling study for improving meteorological inputs for air-quality models. Proc. Twenty-fourth Gulf of Mexico Information Transfer Meeting, U.S. Dept. of the Interior, Minerals Management Service, Gulf of Mexico OCS Region, New Orleans, LA. OCS Study MMS 2008-012, 25-32. [Available online at <http://www.gomr.mms.gov/PDFs/2008/2008-012.pdf>].